

Cite this: *Chem. Sci.*, 2017, 8, 253

Metalloporphyrin-modified semiconductors for solar fuel production†

D. Khusnutdinova, A. M. Beiler, B. L. Wadsworth, S. I. Jacob and G. F. Moore*

We report a direct one-step method to chemically graft metalloporphyrins to a visible-light-absorbing gallium phosphide semiconductor with the aim of constructing an integrated photocathode for light activating chemical transformations that include capturing, converting, and storing solar energy as fuels. Structural characterization of the hybrid assemblies is achieved using surface-sensitive spectroscopic methods, and functional performance for photoinduced hydrogen production is demonstrated *via* three-electrode electrochemical testing combined with photoproduct analysis using gas chromatography. Measurements of the total per geometric area porphyrin surface loadings using a cobalt-porphyrin based assembly indicate a turnover frequency ≥ 3.9 H₂ molecules per site per second, representing the highest reported to date for a molecular-catalyst-modified semiconductor photoelectrode operating at the H⁺/H₂ equilibrium potential under 1-sun illumination.

Received 17th June 2016
Accepted 5th August 2016

DOI: 10.1039/c6sc02664h

www.rsc.org/chemicalscience

Introduction

Energy and environmental issues will likely dominate science and society for the next several decades as climate change threatens the wellbeing of the planet.¹ In this scenario, the development of advanced materials and techniques for controlling matter and energy at the nanoscale is receiving increased global attention² as a technological path to restoring a safe operating space for humanity.³ Artificial photosynthesis, which uses concepts inspired by its biological counterpart to produce fuels, is an attractive approach to storing solar energy.⁴ To this end, the immobilization of molecules on semiconductor materials is gaining interest.⁵ Although some recent progress has been made in development of such assemblies,⁶ finding new and more effective ways to interface catalysts to semiconductor surfaces remains a major challenge.⁷

Metalloporphyrins serve important roles in biology and as components in emerging molecular-based materials.⁸ As electrocatalysts, they are capable of chemically transforming protons into hydrogen as well as converting carbon dioxide into carbon monoxide when electrochemically activated in solution or immobilized at a conductive substrate polarized at an appropriate potential. Herein, we report a one-step method to chemically graft metalloporphyrin complexes onto p-type GaP(100), a midsize optical band gap semiconductor that has shown promise in light-emitting-diode technologies and in

applications for solar energy transduction as light capture and conversion components.⁹ The cobalt and iron porphyrin analogs used in this report are prepared *via* a novel synthetic strategy to yield a macrocycle with a pendent 4-vinylphenyl surface attachment group at the β -position of the porphyrin ring structure. This modification allows use of the UV-induced immobilization chemistry of olefins¹⁰ to attach intact metalloporphyrin complexes to the semiconductor surface. While the mechanistic details of the vinyl group attachment chemistry are not settled, molecular binding appears to occur over bridging oxygen atoms on GaP surfaces.^{6b,i,10a}

Results and discussion

Materials preparation

Synthesis of the 4-vinylphenyl functionalized metalloporphyrins is described in detail as ESI.† Preparation of the GaP substrates for subsequent photochemical functionalization using the structurally modified porphyrins begins with buffered hydrofluoric acid treatment to remove the bulk surface oxide layers. The freshly etched wafers are placed into a sealed quartz flask containing an argon-sparged solution of the appropriate porphyrin and illuminated with shortwave UV light (254 nm) for 2 h. The porphyrin-functionalized wafers are then removed from the flask, ultrasonically cleaned, and dried under nitrogen (see Experimental section for details).

Structural characterization

Grazing angle total reflectance Fourier transform infrared (GATR-FTIR) spectra of unmodified GaP(100) substrates following acid treatment are characterized by significant residual surface oxygen coverage, and static water contact

School of Molecular Sciences and the Biodesign Institute Center for Applied Structural Discovery (CASD), Arizona State University, Tempe, AZ 85287-1604, USA. E-mail: gfmoores@asu.edu

† Electronic supplementary information (ESI) available: Molecular synthesis and characterization, surface characterization, photoelectrochemical data. See DOI: 10.1039/c6sc02664h



angles of $<10^\circ$ indicate a dominant coverage by hydrophilic hydroxyl groups (Fig. S13[†]). However, GATR-FTIR absorbance spectra collected using samples following cobalt or iron porphyrin functionalization, yielding CoP-GaP or FeP-GaP (Fig. 1a), are characterized by unique vibrational features corresponding to C=C bond ring modes of the porphyrin, appearing at 1607 cm^{-1} , as well as transitions that are assigned to the $C_\beta\text{-H}$, $C_\alpha\text{-N}$, and $C_\beta\text{-C}_\beta$ vibrations of the macrocycle (Fig. S14 and S15[†]). FTIR spectra of the cobalt and iron porphyrins prior to surface immobilization show similar C=C bond ring modes centered at 1607 cm^{-1} , but also include an additional pronounced peak centered at 1626 cm^{-1} associated with the vinyl C=C bond (Fig. S16[†]). The lack of this pronounced feature at 1626 cm^{-1} in spectra of the metalloporphyrin-modified GaP samples indicates undetectable to no vinyl functionality on the surface, consistent with the proposed mechanism of the vinyl group grafting chemistry on hydroxyl and oxygen-terminated surfaces.^{6b,i,10a-c} Further, the Co-N and Fe-N vibrations observed on the surfaces of the CoP-GaP or FeP-GaP (1001 cm^{-1} and 997 cm^{-1} , respectively) provide compelling evidence that the porphyrin metal centers remain intact following the grafting procedure (Fig. 1b and c). In contrast, the N-H vibration of analogous free-base porphyrins occurs at 966 cm^{-1} (Fig. S7, S8, & S17[†]). The similarity in positions of the nitrogen-metal vibrations observed on the metalloporphyrin-functionalized GaP surfaces with those observed in spectra of analogous non-surface-attached metalloporphyrins indicates the porphyrin metal centers maintain a similar vibrational environment following immobilization. Lastly, spectra of control samples, in which metalloporphyrins without the vinyl group functionality (CoTTP or FeTTP) are used during the photochemical grafting step, show no evidence of porphyrin complexes at the GaP surface.

X-ray photoelectron (XP) spectroscopy provides additional characterization and evidence of successful functionalization.

As compared to spectra obtained using unmodified GaP samples, survey XP spectra of CoP-GaP surfaces show the presence of additional N, Co, and C elements associated with attached cobalt porphyrins, and spectra of FeP-GaP surfaces show the presence of additional N, Fe, and C elements associated with attached iron porphyrins (Fig. S20 & S22[†]). In addition, high-energy resolution Co 2p core level spectra of the CoP-GaP samples show peaks centered at 780.9 eV ($2p_{3/2}$) and 796.7 eV ($2p_{1/2}$) with a 2 : 1 branching ratio (Fig. 1d). The Co $2p_{3/2}$ signal indicates a complex multiplet structure, consistent with the oxidation state +2 and the open-shell (d7) character of the Co ion (Fig. S21[†]). For the FeP-GaP substrates, Fe 2p core level spectra contain features characteristic of Fe^{III} porphyrins, including peaks centered at 710.8 eV ($2p_{3/2}$) and 724.1 eV ($2p_{1/2}$) (Fig. 1e). For both constructs, analysis of the metal 2p and nitrogen 1s spectral intensity ratios yields metal : nitrogen ratios of 1 : 4, indicating no detectable loss of metal from the attached porphyrin units following UV-induced grafting.

Photoelectrochemical measurements

Illumination of CoP-GaP electrodes polarized at 0 V vs. RHE in pH neutral aqueous solutions results in hydrogen generation at an initial rate of $\sim 10\text{ }\mu\text{L min}^{-1}\text{ cm}^{-2}$ (Fig. 2a-d and Table 1). This rate of hydrogen evolution exhibits less than 10% loss of activity over 4 h of photoelectrochemical (PEC) testing (Fig. S27[†]). By contrast, the iron-based constructs show significant diminution of performance during PEC testing, including a rapid loss in current density following illumination during bulk-electrolysis measurements (Fig. 2a). Further, the relatively stable photocurrent densities that are measured after the drop off are similar in value to those initially achieved using unmodified GaP electrodes polarized at the same potential (0 V vs. RHE). Thus, there is a nearly complete loss of the photocurrent gains afforded by FeP functionalization. Although iron

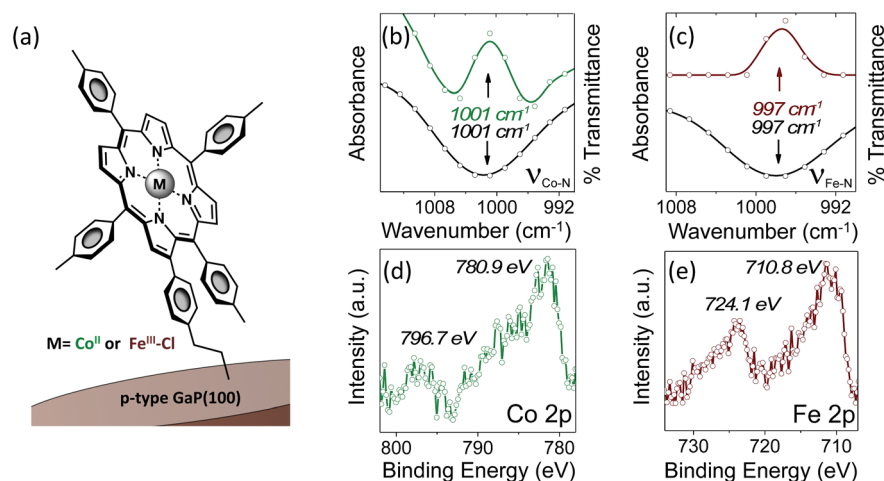


Fig. 1 (a) Schematic representation of the CoP-GaP and FeP-GaP constructs. (b) GATR-FTIR absorbance spectra showing the porphyrin pyrrolic nitrogen-cobalt vibration, $\nu_{\text{Co-N}}$, at the surface of CoP-GaP (green) and FTIR transmission spectra showing the $\nu_{\text{Co-N}}$ of the non-surface-attached cobalt porphyrin (black). (c) GATR-FTIR absorbance spectra showing the porphyrin pyrrolic nitrogen-iron vibration, $\nu_{\text{Fe-N}}$, at the surface of FeP-GaP (dark red) and FTIR transmission spectra showing the $\nu_{\text{Fe-N}}$ of the non-surface-attached iron porphyrin (black). (d) Co 2p core level XP spectra of CoP-GaP. (e) Fe 2p core level XP spectra of FeP-GaP.



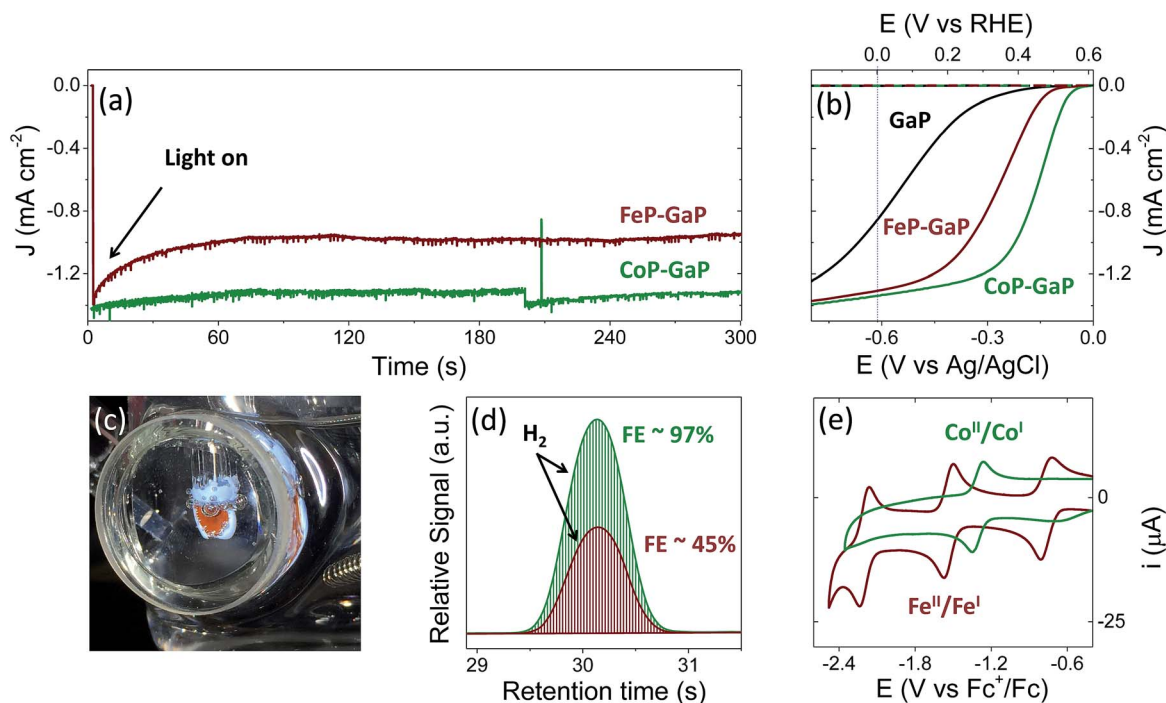


Fig. 2 Three-electrode electrochemical data collected using unmodified GaP(100) (black), CoP-GaP (green), or FeP-GaP (dark red) working electrodes in phosphate buffer (pH 7) including (a) chronoamperograms using working electrodes polarized at a constant potential of 0 V vs. RHE and under 1-sun illumination (100 mW cm^{-2}), (b) linear sweep voltammograms recorded in the dark (dashed) or under 1-sun illumination (solid), (c) an image of a CoP-GaP photocathode under photoelectrochemical testing, and (d) gas chromatograms obtained using samples of head-space gas collected from sealed photoelectrochemical cells containing working electrodes polarized at a constant potential of 0 V vs. RHE and under 1-sun illumination. The amount of hydrogen produced in these experiments corresponds to a faradaic efficiency (FE) of 97% following 30 min of illumination using CoP-GaP and 45% following 6 min of illumination using FeP-GaP. (e) Cyclic voltammetry data recorded using butyronitrile solutions of model cobalt (green) or iron (dark red) porphyrin compounds are included for comparison.

porphyrins are notorious for their relative instability, including a propensity to form μ -oxo dimers and undergo auto-reduction reactions,^{89,11} a detailed analysis of the photocurrent degradation pathways regarding the FeP-GaP constructs is currently unavailable. These results do, however, illustrate the synthetic versatility of the porphyrin architecture, including selection of the catalytic metal site for controlling activity, and presence of ligand auxiliaries for tailoring their molecular structure as well as associated electronic properties.

During PEC testing, the formation of gas bubbles at the surface of the porphyrin-modified electrode are transiently observed in linear sweep voltammetry experiments, when the electrodes are polarized at potentials generating cathodic currents, and continuously observed during bulk photoelectrolysis experiments (Fig. 2c). Gas chromatography analysis of the photoproducts confirms the production of hydrogen with

near-unity faradaic efficiency (measured at $\sim 97\%$ following 30 min of illumination) when using CoP-GaP working electrodes (Fig. 2d). These results confirm that no measurable hydrogen is present prior to illumination of the electrode surface (Fig. S24†) and the rate of hydrogen production is directly correlated with the current produced by the cell during illumination. Measurements performed using FeP-GaP working electrodes polarized at 0 V vs. RHE also confirm the photoproduction of hydrogen. However, the faradaic efficiency is $\sim 45\%$ following 6 min of illumination.

To facilitate comparisons with data obtained using the metalloporphyrin-modified GaP constructs in aqueous conditions, cyclic voltammograms of CoTTP and FeTTP recorded in organic solvents with a supporting electrolyte (0.1 M tetrabutylammonium hexafluorophosphate in butyronitrile) are included in this report (Fig. 2e). Under these conditions, the difference in potential between the midpoints of the $\text{Co}^{\text{II}}/\text{Co}^{\text{I}}$ and $\text{Fe}^{\text{II}}/\text{Fe}^{\text{I}}$ couples is 230 mV, with the cobalt relay occurring at less negative potentials (Table S1†). For the metalloporphyrin-modified GaP surfaces, a difference in potential to access the catalytically active cobalt or iron redox state in aqueous conditions may contribute to the 120 mV offset required to achieve a -1 mA cm^{-2} current density using the CoP-GaP versus FeP-GaP photocathodes (Table 1). However, other factors, including differences in hydricity of the metal centers¹² and possible changes in electronic structure of the underlying semiconductors upon functionalization¹³ may

Table 1 PEC characteristics of GaP, CoP-GaP, and FeP-GaP photocathodes

Construct	V_{oc} (V vs. RHE)	E at -1 mA cm^{-2} (V vs. RHE)	J at 0 V vs. RHE (mA cm^{-2})
GaP	0.57 ± 0.03	-0.04 ± 0.06	-0.86 ± 0.21
CoP-GaP	0.61 ± 0.01	0.35 ± 0.03	-1.31 ± 0.03
FeP-GaP	0.61 ± 0.01	0.23 ± 0.07	-1.29 ± 0.04



contribute to this divergence. Nonetheless, the saturating current densities, measured at 0 V vs. RHE using CoP–GaP working electrodes, do increase approximately linearly with illumination intensity (Fig. 3), indicating that photocarrier transport to the interface in part limits the performance and that improvement in the spectral coverage and photophysical properties of the underpinning semiconductor could yield additional efficiency gains.

A comparison of the photon flux striking the CoP–GaP surface at simulated 1-sun intensity (Fig. 3 & S29†) with the electron flux measured during PEC testing allows an analysis of external quantum efficiency (EQE). Considering only photons in the GaP actinic range (Fig. S11 & S12†), *i.e.* those with energies higher than the 2.26 eV GaP band gap, the EQE = 19% for CoP–GaP electrodes polarized at 0 V vs. RHE. A similar analysis of the optical to chemical power conversion efficiency (η)^{14a} is achieved by comparing the spectral irradiance at this wavelength range with the output chemical power represented by the rate of hydrogen production. Using the enthalpy of H₂ combustion (286 kJ mol⁻¹) or change in Gibb's free energy (237 kJ mol⁻¹), $\eta = 11%$ or 9%, respectively. We emphasize that these measurements are performed using a three-electrode configuration^{14b} and thus represent energetics and efficiencies associated with a photocathode component, not a device.

Total cobalt loadings on the CoP–GaP surface were obtained using inductively coupled plasma mass spectroscopy (ICP-MS) (see Experimental section for details), yielding a cobalt porphyrin surface concentration of 0.59 ± 0.03 nmol cm⁻². The loadings obtained from this analysis combined with the current densities measured in polarization experiments using CoP–GaP working electrodes yield information on the activity of the electrodes per number of porphyrins assembled on the surface and thus an estimate of the immobilized porphyrin turnover frequency (TOF). Using only the increase in current density obtained for a GaP electrode polarized at 0 V vs. RHE following cobalt porphyrin surface functionalization, this equates to a TOF ≥ 3.9 H₂ molecules site⁻¹ s⁻¹, representing the highest reported to date for a molecular-catalyst-modified semiconductor photoelectrode operating at the H⁺/H₂ equilibrium potential under 1-sun illumination. In future work, implementation of porphyrins with improved catalytic features and the development of synthetic methodologies to achieve higher porphyrin surface loading as well as improved interfacial dynamics may lead to further performance gains.

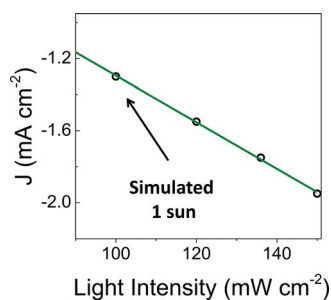


Fig. 3 Photocurrent density recorded at increasing illumination intensity using a CoP–GaP working electrode polarized at 0 V vs. RHE.

Conclusions

We describe a one-step method to chemically graft metal-porphyrin catalysts onto p-type gallium phosphide (100). The porphyrin complexes are structurally modified with a 4-vinyl-phenyl group essential to successful semiconductor attachment using the UV-induced grafting method. Structural analysis of the constructs using surface-sensitive characterization techniques, including XP and GATR-FTIR spectroscopy, provides evidence of successful grafting. The resulting hybrid material can be used as a photocathode for driving the hydrogen evolution half-reaction and shows significantly improved photoelectrochemical performance over unmodified electrodes. When using GaP(100) with identical doping conditions (*i.e.* cut from the same ingot), the PEC results using CoP–GaP show an enhanced rate and stability of photoinduced hydrogen production over the analogous FeP–GaP assemblies as well as those previously reported^{6j} using cobaloxime-polymer-modified GaP electrodes prepared using a two-step attachment chemistry (Fig. S28†). Unlike the cobaloximes,¹⁵ the Co and Fe porphyrins permit access to metal^I/metal⁰ redox couples and are known catalysts for the electrochemical reduction of carbon dioxide.⁸ Thus, methods to covalently graft metalloporphyrins to semiconductor substrates could lead to new perspectives and approaches of photoelectrochemically activating carbon dioxide. In addition, the porphyrins are synthetically versatile, allowing tailoring of their molecular structure and electronic properties as new discoveries and material developments emerge. Key features of the constructs reported here include use of metalloporphyrins with built-in chemical sites for direct grafting to a GaP semiconductor, creating hybrid assemblies capable of converting photonic energy to fuel.

Experimental

Materials and synthesis

All compounds were synthesized from commercially available starting materials (see ESI† Molecular synthesis and characterization). All reagents were purchased from Aldrich. Solvents were obtained from Aldrich or Mallinckrodt. Dichloromethane, hexanes, toluene and p-tolyl aldehyde were freshly distilled before use. Milli-Q water (18.2 MΩ cm) was used to prepare all aqueous solutions.

Single crystalline p-type gallium phosphide wafers were purchased from University Wafers. The material is single side polished to an epi-ready finish. The p-type Zn-doped GaP(100) wafers have a resistivity of 0.2 Ω cm, a mobility of 66 cm² V⁻¹ s⁻¹, and a carrier concentration of 4.7×10^{17} cm⁻³, with an etch pit density of less than 8×10^4 cm⁻².

Wafer cleaning procedure

Diced semiconductor samples were degreased by wiping the surface with an acetone soaked cotton swab and ultrasonically cleaning in acetone and isopropanol for 5 min each, followed by drying under nitrogen. Samples were then exposed to an air-generated oxygen plasma (Harrick Plasma, U.S.) at 30 W for



2 min. Surface oxide layers were then removed by immersion of the plasma-treated samples in buffered hydrofluoric acid (6 : 1 HF/NH₄F in H₂O) for 5 min, followed by rinsing with Milli-Q water.

Wafer functionalization

Freshly etched wafers were put into an argon-sparged solution of the appropriate porphyrin (1 mM) in toluene and exposed to 254 nm UV light for 2 h. After thoroughly rinsing with toluene the wafers were dried under nitrogen and stored under vacuum.

Electrode fabrication

GaP working electrodes were fabricated by applying an indium-gallium eutectic (Aldrich) to the backside of a wafer, then fixing a copper wire to the back of the wafer using a conductive silver epoxy (Circuit Works). The copper wire was passed through a glass tube, and the wafer was insulated and attached to the glass tube with Loctite 615 Hysol Epoxi-patch adhesive. The epoxy was allowed to fully cure before testing the electrodes.

Instrument descriptions and experimental details

UV-Vis. Ultraviolet-visible (UV-Vis) optical spectra were recorded on a Shimadzu SolidSpec-3700 spectrometer with a D₂ (deuterium) lamp for the ultraviolet range and a WI (halogen) lamp for the visible and near-infrared. Transmission and reflectance measurements were performed with an integrating sphere.

Mass spectra. Mass spectra of all compounds were obtained with Voyager DE STR matrix-assisted laser desorption/ionization time-of-flight spectrometer (MALDI-TOF) mass spectrometer in positive ion mode employing a *trans,trans*-1,4-diphenyl-1,3-butadiene matrix (unless otherwise noted). The reported mass is for the most abundant isotopic ratio observed (obsd.). To facilitate comparison, calculated values of the anticipated most abundant isotopic ratio (calc.) are listed before the experimental result.

NMR. Nuclear magnetic resonance (NMR) spectra were recorded on a Varian NMR spectrometer operating at 400 MHz. Unless otherwise stated, all spectra were collected at room temperature.

FTIR. Grazing angle attenuated total reflection Fourier transform infrared spectroscopy (GATR-FTIR) was performed using a VariGATR accessory (Harrick Scientific) with a Ge crystal plate installed in a Bruker Vertex 70. A minimum of 4 individual wafers were tested for each sample. Samples were pressed against the Ge crystal to ensure effective optical coupling. Spectra were collected under a dry nitrogen purge with a 4 cm⁻¹ resolution, GloBar MIR source, a broadband KBr beamsplitter, and a liquid nitrogen cooled MCT detector. Background measurements were obtained from the bare Ge crystal and the data were processed using OPUS software. Spectra from model compounds in pressed KBr pellets were acquired with the same settings but using transmission mode. GATR measurements were baseline corrected for rubberband scattering.

XPS. X-ray photoelectron spectroscopy (XPS) was performed using a monochromatized Al K α source ($h\nu = 1486.6$ eV),

operated at 63 W, on a Kratos system at a takeoff angle of 0° relative to the surface normal and a pass energy for narrow scan spectra of 20 eV at an instrument resolution of approximately 700 meV. Survey spectra (40 scans) were collected with a pass energy of 150 eV. A minimum of 2 wafers were analyzed for each sample. Spectral fitting was performed using Casa XPS analysis software and all spectra were calibrated by adjusting C 1s core level position to 284.8 eV. Curves were fit with quasi-Voigt lines following Shirley background subtraction.

Electrochemistry. Cyclic voltammetry was performed with a Biologic potentiostat using a glassy carbon (3 mm diameter) disk, a platinum counter electrode, and a silver wire pseudoreference electrode in a conventional three-electrode cell at a scan rate of 250 mV s⁻¹. Anhydrous dimethylformamide or butyronitrile (Aldrich) was used as the solvent for electrochemical measurements. The supporting electrolyte was 0.1 M tetrabutylammonium hexafluorophosphate. The solution was sparged with argon. The working electrode was cleaned between experiments by polishing with alumina (50 nm diameter) slurry, followed by solvent rinses.

Photoelectrochemistry. Photoelectrochemical (PEC) testing was performed using 100 mW cm⁻² illumination from a 100 W Oriol Solar Simulator equipped with an AM 1.5 filter. Linear sweep voltammetry and three-electrode electrolysis (chronoamperometry) were performed with a Biologic potentiostat using a platinum coil counter electrode, a Ag/AgCl, NaCl (3 M) reference electrode (0.21 V vs. NHE), and GaP working electrodes (including GaP following buffered HF treatment, cobalt porphyrin-modified GaP, and iron porphyrin-modified GaP) in a modified cell containing a quartz window. A minimum of 4 individual wafers were tested for each sample. The supporting electrolyte was 0.1 M phosphate buffer (pH 7). Linear sweep voltammograms were recorded at sweep rates of 100 mV s⁻¹ under a continuous flow of 5% hydrogen in nitrogen. Open-circuit photovoltages were determined by the zero current value in the linear sweep voltammograms. Chronoamperometry was performed with the working electrode polarized at 0 V vs. RHE, where E vs. RHE = E vs. NHE + 0.05916 V \times pH = E vs. Ag/AgCl + 0.05916 V \times pH + 0.21 V.

GC. Gas analysis was performed *via* gas chromatography (GC) using an Agilent 490 Micro GC equipped with a 5 Å Mol-Sieve column at a temperature of 80 °C and argon as the carrier gas. Gas samples were syringe injected using 5 mL aliquots of headspace gas collected with a gas-tight Hamilton syringe from a sealed PEC cell both prior to and following 30 min of three-electrode photoelectrolysis using a cobalt porphyrin-modified working electrode polarized at 0 V vs. RHE or following 6 min of three-electrode photoelectrolysis using an iron porphyrin-modified working electrode polarized at 0 V vs. RHE. Prior to the experiment the cell was purged for 30 min with argon before sealing. The retention time of hydrogen was confirmed using a known source of hydrogen obtained from a standard lecture bottle containing a hydrogen and argon mixture. In Fig. 2d, the relative signal intensity is based on the ratio of total hydrogen molecules produced to half the number of net electrons passed from the counter to the working electrode. Thus, the signal areas are representative of the relative faradaic efficiencies for hydrogen production.



ICP-MS. Inductively coupled plasma mass spectroscopy (ICP-MS) was performed on a Thermo-Finnigan Neptune ICP-MS. The samples were run in kinetic-energy discrimination (KED) mode. The ICP-MS samples were prepared by immersing a CoP-GaP wafer into 1000 μL of concentrated Omni trace H_2SO_4 solution and heating the solution at 60 $^\circ\text{C}$ for 20 min, followed by sonicating the solution for 1 h. The solution was then diluted to 0.5 M H_2SO_4 by taking 108 μL of the 1000 μL solution and diluting to 4000 μL . Three different wafers of CoP-GaP were analyzed. Unfunctionalized GaP substrates were analyzed as controls. The trace amounts of cobalt in these controls were averaged and subtracted from the CoP-GaP cobalt concentrations.

Acknowledgements

This work was supported by The College of Liberal Arts and Sciences at Arizona State University, the Biodesign Institute Center for Applied Structural Discovery (CASD) and LightWorks. We thank Gwyneth Gordon for assistance with ICP-MS measurements and Timothy Karcher for assistance with XP data collection. A. M. B. and B. L. W gratefully acknowledge IGERT-SUN fellowships funded by the National Science Foundation (Award 1144616). NMR studies were performed using the Magnetic Resonance Research Center at Arizona State University.

Notes and references

- 1 IPCC 5th Assessment Report, Geneva, Switzerland, 2014.
- 2 T. A. Faunce, W. Lubitz, A. W. Rutherford, D. MacFarlane, G. F. Moore, P. Yang, D. G. Nocera, T. A. Moore, D. H. Gregory, S. Fukuzumi and K. B. Yoon, *Energy Environ. Sci.*, 2013, **6**, 695.
- 3 (a) J. Rockström, W. Steffen, K. Noone, Å. Persson, F. S. Chapin, E. F. Lambin, T. M. Lenton, M. Scheffer, C. Folke, H. J. Schellnhuber and B. Nykvist, *Nature*, 2009, **461**, 472; (b) W. Steffen, K. Richardson, J. Rockström, S. E. Cornell, I. Fetzer, E. M. Bennett, R. Biggs, S. R. Carpetner, W. de Vries, C. A. de Wit, C. Folke, D. Gerten, J. Heinke, G. M. Mace, L. M. Persson, V. Ramanathan, B. Reyers and S. Sörlin, *Science*, 2015, **347**, 736.
- 4 (a) A. J. Bard and M. A. Fox, *Acc. Chem. Res.*, 1995, **28**, 141; (b) G. F. Moore and G. W. Brudvig, *Annu. Rev. Condens. Matter Phys.*, 2011, **2**, 303; (c) R. E. Blankenship, D. M. Tiede, J. Barber, G. W. Brudvig, G. Fleming, M. Ghirardi, M. R. Gunner, W. Junge, D. M. Kramer, A. Melis and T. A. Moore, *Science*, 2011, **332**, 805; (d) P. D. Tran, L. H. Wong, J. Barber and J. S. C. Loo, *Energy Environ. Sci.*, 2012, **5**, 5902; (e) J. R. Swierk and T. E. Mallouk, *Chem. Soc. Rev.*, 2013, **42**, 2357; (f) D. G. Nocera, *Acc. Chem. Res.*, 2012, **45**, 767.
- 5 M. G. Walter, E. L. Warren, J. R. McKone, S. W. Boettcher, Q. Mi, E. A. Santori and N. S. Lewis, *Chem. Rev.*, 2010, **110**, 6446.
- 6 (a) N. Queyriaux, N. Kaeffer, A. Morozan, M. Chavarot-Kerlidou and V. Artero, *J. Photochem. Photobiol., C*, 2015, **25**, 90; (b) A. Krawicz, J. Yang, E. Anzenberg, J. Yano, I. D. Sharp and G. F. Moore, *J. Am. Chem. Soc.*, 2013, **135**, 11861; (c) A. Krawicz, D. Cedeno and G. F. Moore, *Phys. Chem. Chem. Phys.*, 2014, **16**, 15818; (d) D. Cedeno, A. Krawicz, P. Doak, M. Yu, J. B. Neaton and G. F. Moore, *J. Phys. Chem. Lett.*, 2014, **5**, 3222; (e) C. A. Downes and S. C. Marinescu, *J. Am. Chem. Soc.*, 2015, **137**, 13740; (f) H. J. Kim, J. Seo and M. J. Rose, *ACS Appl. Mater. Interfaces*, 2016, **8**, 1061; (g) J. Gu, Y. Yan, J. L. Young, K. X. Steirer, N. R. Neale and J. A. Turner, *Nat. Mater.*, 2015, **15**, 456; (h) M. Schreier, J. Luo, P. Gao, T. Moehl, T. M. Mayer and M. Grätzel, *J. Am. Chem. Soc.*, 2016, **138**, 1938; (i) A. M. Beiler, D. Khusnutdinova, S. I. Jacob and G. F. Moore, *ACS Appl. Mater. Interfaces*, 2016, **8**, 10038; (j) A. M. Beiler, D. Khusnutdinova, S. I. Jacob and G. F. Moore, *Ind. Eng. Chem. Res.*, 2016, **55**, 5306.
- 7 J. R. McKone, S. C. Marinescu, B. S. Brunschwig, J. R. Winkler and H. B. Gray, *Chem. Sci.*, 2014, **5**, 865.
- 8 (a) W. Auwärter, D. Ćija, F. Klappenberger and J. V. Barth, *Nat. Chem.*, 2015, **7**, 105; (b) A. J. Morris, G. J. Meyer and E. Fujita, *Acc. Chem. Res.*, 2009, **42**, 1983; (c) A. Maurin and M. Robert, *J. Am. Chem. Soc.*, 2016, **138**, 2492; (d) S. Lin, C. S. Diercks, Y. B. Zhang, N. Kornienko, E. M. Nichols, Y. Zhao, A. R. Paris, D. Kim, P. Yang, O. M. Yaghi and C. J. Chang, *Science*, 2015, **349**, 1208; (e) M. L. Rigsby, D. J. Wasylenko, M. L. Pegis and J. M. Mayer, *J. Am. Chem. Soc.*, 2015, **137**, 4296; (f) J. R. Swierk, D. D. Méndez-Hernández, N. S. McCool, P. Liddell, Y. Terazono, I. Pahlk, J. J. Tomlin, N. V. Oster, T. A. Moore, A. L. Moore, D. Gust and T. E. Mallouk, *Proc. Natl. Acad. Sci. U. S. A.*, 2015, **112**, 1681; (g) C. Costentin, M. Robert and J.-M. Savéant, *Acc. Chem. Res.*, 2015, **48**, 2996; (h) S. R. Ahrenholtz, C. C. Epley and A. J. Morris, *J. Am. Chem. Soc.*, 2014, **136**, 2464; (i) S. A. Yao, R. E. Ruther, L. Zhang, R. A. Franking, R. J. Hamers and J. F. Berry, *J. Am. Chem. Soc.*, 2012, **134**, 15632; (j) D. J. Sommer, M. D. Vaughn and G. Ghirlanda, *Chem. Commun.*, 2014, **50**, 15852; (k) G. F. Moore, J. D. Blakemore, R. L. Milot, J. F. Hull, H. E. Song, L. Cai, C. A. Schmuttenmaer, R. H. Crabtree and G. W. Brudvig, *Energy Environ. Sci.*, 2011, **4**, 2389; (l) G. F. Moore, M. Hamburger, M. Gervaldo, O. G. Poluektov, T. Rajh, D. Gust, T. A. Moore and A. L. Moore, *J. Am. Chem. Soc.*, 2008, **130**, 10466; (m) J. S. Lindsey and D. F. Bocian, *Acc. Chem. Res.*, 2011, **44**, 638; (n) T. Dhanasekaran, J. Grodkowski, P. Neta, P. Hambright and F. Etsuko, *J. Phys. Chem. A*, 1999, **103**, 7742; (o) J.-M. Savéant, *Chem. Rev.*, 2008, **108**, 2348; (p) D. Lexa, J. Mispelter and J.-M. Savéant, *J. Am. Chem. Soc.*, 1981, **103**, 6806; (q) A. R. Oveisi, K. Zhang, A. Khorramabadi-zad, O. K. Farha and J. T. Hupp, *Sci. Rep.*, 2015, **5**, 10621; (r) Z. Weng, J. Jiang, Y. Wu, Z. Wu, X. Guo, K. L. Materna, W. Liu, V. S. Batista, G. W. Brudvig and H. Wang, *J. Am. Chem. Soc.*, 2016, **138**, 8076–8079; (s) M. R. Civic and P. H. Dinolfo, *ACS Appl. Mater. Interfaces*, 2016, **8**, 20465; (t) I. Hod, M. D. Sampson, P. Deria, C. P. Kubiak, O. K. Farha



- and J. T. Hupp, *ACS Catal.*, 2015, **5**, 6302; (u) B. Kumar, M. Llorente, J. Froehlich, T. Dang, A. Sathrum and C. P. Kubiak, *Annu. Rev. Phys. Chem.*, 2012, **63**, 541; (v) S. Ardo, D. Achey, A. J. Morris, M. Abrahamsson and G. J. Meyer, *J. Am. Chem. Soc.*, 2011, **133**, 16572.
- 9 (a) M. Halmann, *Nature*, 1978, **275**, 115; (b) M. Grätzel, *Nature*, 2001, **414**, 338; (c) C. Liu, N. P. Dasgupta and P. Yang, *Chem. Mater.*, 2014, **26**, 415; (d) B. Kaiser, D. Fertig, J. Ziegler, J. Klett, S. Hoch and W. Jaegermann, *ChemPhysChem*, 2012, **13**, 3053; (e) E. E. Barton, D. M. Rampulla and A. B. Bocarsly, *J. Am. Chem. Soc.*, 2008, **130**, 6342; (f) M. J. Price and S. Maldonado, *J. Phys. Chem. C*, 2009, **113**, 11988; (g) G. Zeng, J. Qiu, Z. Li, P. Pavaskar and S. B. Cronin, *ACS Catal.*, 2014, **4**, 3512; (h) A. Standing, S. Assali, L. Gao, M. A. Verheijen, D. van Dam, Y. Cui, P. H. L. Notten, J. E. M. Haverkort and E. P. A. M. Bakkers, *Nat. Commun.*, 2015, **6**, 7824; (i) J. Sun, C. Liu and P. Yang, *J. Am. Chem. Soc.*, 2011, **133**, 19306; (j) C. Liu, J. Sun, J. Tang and P. Yang, *Nano Lett.*, 2012, **12**, 5407.
- 10 (a) G. F. Moore and I. D. Sharp, *J. Phys. Chem. Lett.*, 2013, **4**, 568; (b) R. Franking, E. C. Landis, H. Kim and R. J. Hamers, *ACS Appl. Mater. Interfaces*, 2009, **1**, 1013; (c) D. Richards, D. Zemlyanov and A. Ivanisevic, *Langmuir*, 2010, **18**, 10676; (d) M. Seifert, A. H. R. Koch, F. Deubel, T. Simmet, L. A. Hess, M. Stutzmann, R. Jordan, J. A. Garrido and I. D. Sharp, *Chem. Mater.*, 2013, **25**, 466; (e) M. Steenackers, A. M. Gigler, N. Zhang, F. Deubel, M. Seifert, L. H. Hess, C. H. Lim, K. P. Loh, J. A. Garrido, R. Jordan, M. Stutzmann and I. D. Sharp, *J. Am. Chem. Soc.*, 2011, **133**, 10490; (f) R. L. Cicero, M. R. Linford and C. E. D. Chidsey, *Langmuir*, 2000, **16**, 5688.
- 11 (a) K. Shin, S. K. Kramer and H. M. Goff, *Inorg. Chem.*, 1987, **26**, 4103; (b) S. Modi, V. P. Shedbalkar and D. V. Behere, *Inorg. Chim. Acta*, 1990, **173**, 9; (c) A. L. Balch, B. C. Noll, M. M. Olmstead and S. L. Phillips, *Inorg. Chem.*, 1996, **35**, 6495; (d) T. N. St. Claire and A. L. Balch, *Inorg. Chem.*, 1999, **38**, 684.
- 12 (a) D. L. DuBois and D. E. Berning, *Appl. Organomet. Chem.*, 2000, **14**, 860; (b) C. Creutz and M. H. Chou, *J. Am. Chem. Soc.*, 2009, **131**, 2794; (c) S. J. Connelly, E. S. Wiedner and A. M. Appel, *Dalton Trans.*, 2015, **44**, 5933.
- 13 (a) M. Barroso, A. J. Cowan, S. R. Pendlebury, M. Gratzel, D. R. Klug and J. R. Durrant, *J. Am. Chem. Soc.*, 2011, **133**, 14868; (b) B. Klahr, S. Gimenez, F. Fabregat-Santiago, T. Hamann and J. Bisquert, *J. Am. Chem. Soc.*, 2012, **134**, 4294; (c) F. Lin and S. W. Boettcher, *Nat. Mater.*, 2013, **13**, 81; (d) M. M. Waagele, X. Chen, D. M. Herlihy and T. Cuk, *J. Am. Chem. Soc.*, 2014, **136**, 10632; (e) J. E. Thorne, S. Li, C. Du, G. Qin and D. Wang, *J. Phys. Chem. Lett.*, 2015, **6**, 4083.
- 14 (a) A. Nozik, *Nature*, 1975, **257**, 383–386; (b) Z. Chen, T. Jaramillo, T. G. Deutsch, A. Kleiman-Shwarsstein, A. J. Forman, N. Gaillard, R. Garland, K. Takane, C. Heske, M. Sunkara, E. W. McFarland, K. Domen, E. L. Miller, J. A. Turner and H. N. Dinh, *J. Mater. Res.*, 2010, **25**, 3.
- 15 (a) S. R. Soltau, J. Niklas, P. D. Dahlberg, O. G. Poluektov, D. M. Tiede, K. L. Mulfort and L. M. Utschig, *Chem. Commun.*, 2015, **51**, 10628; (b) D. W. Wakerley and E. Reisner, *Phys. Chem. Chem. Phys.*, 2014, **16**, 5739; (c) B. S. Veldkamp, W.-S. Han, S. M. Dyar, S. W. Eaton, M. A. Ratner and M. R. Wasielewski, *Energy Environ. Sci.*, 2013, **6**, 1917; (d) E. S. Andreiadis, P.-A. Jacques, P. D. Tran, A. Leyris, M. Chavarot-Kerlidou, B. Jusselme, M. Matheron, J. Pécaut, S. Palacin, M. Fontecave and V. Artero, *Nat. Chem.*, 2012, **5**, 48; (e) S. C. Marinescu, J. R. Winkler and H. B. Gray, *Proc. Natl. Acad. Sci. U. S. A.*, 2012, **109**, 15127; (f) L. Li, L. Duan, F. Wen, C. Li, M. Wang, A. Hagfeldt and L. Sun, *Chem. Commun.*, 2012, **48**, 988; (g) C. C. L. McCrory, C. Uyeda and J. C. Peters, *J. Am. Chem. Soc.*, 2012, **134**, 3164; (h) F. Lakadamyali, A. Reynal, M. Kato, J. Durrant and E. Reisner, *Chem.–Eur. J.*, 2012, **18**, 15464; (i) J. T. Muckerman and E. Fujita, *Chem. Commun.*, 2011, **47**, 12456; (j) B. H. Solis and S. Hammes-Schiffer, *Inorg. Chem.*, 2011, **50**, 11252; (k) J. L. Dempsey, B. S. Brunschwig, J. R. Winkler and H. B. Gray, *Acc. Chem. Res.*, 2009, **42**, 1995; (l) P. Du, K. Knowles and R. Eisenberg, *J. Am. Chem. Soc.*, 2008, **130**, 12576; (m) C. Baffert, V. Artero and M. Fontecave, *Inorg. Chem.*, 2007, **46**, 1817; (n) X. Hu, B. M. Cossairt, B. S. Brunschwig, N. S. Lewis and J. C. Peters, *Chem. Commun.*, 2005, 4723; (o) M. Razavet, V. Artero and M. Fontecave, *Inorg. Chem.*, 2005, **44**, 4786; (p) X. Hu, B. S. Brunschwig and J. C. Peters, *J. Am. Chem. Soc.*, 2007, **129**, 8988; (q) P. Connelly and J. H. Espenson, *Inorg. Chem.*, 1986, **25**, 2684.

